

Modeling and Loop Shaping of Single-Joint Amplification Exoskeleton with Contact Sensing and Series Elastic Actuation

Binghan He¹, Gray C. Thomas, Nicholas Paine and Luis Sentis

Abstract—In this paper we consider a class of exoskeletons designed to amplify the strength of humans through feedback of sensed human-robot interactions and actuator forces. We define an amplification error signal based on a reference amplification rate, and design a linear feedback compensator to attenuate this error. Since the human operator is an integral part of the system, we design the compensator to be robust to both a realistic variation in human impedance and a large variation in load impedance. We demonstrate our strategy on a one-degree of freedom amplification exoskeleton connected to a human arm, following a three dimensional matrix of experimentation: slow or fast human motion; light or extreme exoskeleton load; and soft or clenched human arm impedances. We demonstrate that a slightly aggressive controller results in a borderline stable system—but only for soft human musculoskeletal behavior and a heavy load. This class of exoskeleton systems is interesting because it can both amplify a human’s interaction forces—so long as the human contacts the environment through the exoskeleton—and attenuate the operator’s perception of the exoskeleton’s reflected dynamics at frequencies within the bandwidth of the control.

I. INTRODUCTION

Long the purview of science fiction, exoskeletons are quickly becoming a modern reality—augmenting the strength of healthy operators as they walk and interact with the world. A vast literature catalogs the breadth and history of the exoskeleton concept, with survey papers offering disambiguation between such exoskeletons and the orthotic systems designed for medical purposes [1], and between “parallel-limb exoskeletons for load transfer” such as our type of system, and several other types that aim to help the human in a different sense [2] (by reducing the metabolic cost of walking, for example [3]). Amplification exoskeletons, like the concept of a “Human Extender” [4], interact with the world and the human operator at the same time, with the world perceiving a strengthened operator, while the operator in feeling a weakened world and a lighter exoskeleton, all through the feedback action of the device in response to force-sensors embedded at the human–robot interface.

With the human maintaining full control over the motion of the amplification exoskeleton, their primary challenge is not so much autonomy as stable feedback control in

This work was supported by the U.S. Government and NASA Space Technology Research Fellowship NNX15AQ33H. We thank the members of the Human Centered Robotics Lab, University of Texas at Austin and Aptronik Systems Inc who provided insight and expertise that assisted the research. Authors are with The Departments of Mechanical Engineering (B.H., G.C.T.) and Aerospace Engineering (L.S.), University of Texas at Austin, Austin, TX and with Aptronik Systems Inc (N.P.), Austin, TX. Send correspondence to ¹binghan at utexas dot edu.

the presence of the difficult-to-model human and the uncertain environment. Humans possess naturally adjustable compliance properties which depend on muscle activation [5]. The methodology of interaction controller design [6] has had success modeling humans as active systems which are passive except for non-state-dependent biases. Robust robot impedance [7] and haptic interface [8], [9] controller design strategies have supported and used this model to great effect, while acknowledging its conservatism. The task of amplification exoskeletons, however, is to emulate a reduction in mass. This can be achieved stably if the human model is more precisely known [10] than just a passive assumption but is acknowledged to be a challenging problem.

One of the earliest known amplification-oriented exoskeleton is the hulking machine HARDIMAN I [11], which introduced the world to the control challenges of exoskeletons, as it was never safe enough to power on both upper and lower body with an operator. Ref. [4], much later, conceived of extenders for industrial use with operators controlling much larger machines through force-sensitive interfaces—acknowledging a tradeoff between stability and performance both in linear and robust-nonlinear models [4]. Ref. [12] defined a performance criterion for such extenders using a matrix of amplification-levels; a critical frequency, since such amplification cannot be maintained at all frequencies; and introduced a stability filter that allowed the device to ensure robustness to varied operator behavior. However, the later BLEEX exoskeleton from the same lab was not designed in this framework due to practical issues with force sensors [13] and the discovery of an alternative strategy using high sensitivity cancellation of the natural exoskeleton dynamics—which accomplished an apparent-mass reduction without the force sensors, at the cost of no longer amplifying human-world interaction forces (and extreme sensitivity to the dynamic model) [14].

The strategy of measuring a network of force sensors on the human alone, using them to determine human intent, and then using a simulated ideal reaction to this intent as input to a position controller is known as admittance control, and it represents a slight departure from the human extender ideal: accurate reflection of the environmental forces to the human takes a backseat, since there are no force sensors for the environment. This is a very successful paradigm—at least in the absence of environmental contact—it works for giant gantry robots [15], complex upper body robots [16], the slow-yet-amplifying (full-) body extender [17], and the Sarcos-Ratheon exoskeleton described indirectly in their 2014 Patent [18]—which is implied to be hydraulic,

TABLE I: List of Symbols

Symbol	Meaning (Space)	Symbol	Meaning (Space)
K_h, B_h, M_h	Human stiffness, damping and inertia (rotary)	τ_c, f_c	Contact torque (rotary) and force (linear)
k_h, b_h, m_h, Z_h	Human stiffness, damping, inertia and impedance (linear)	ω_h, ζ_h	Natural frequency and damping ratio of Z_h
$\bar{M}_e, \bar{M}_e, M_e$	Inertias of exoskeleton, load and combined (rotary)	α, f_α	Amplification factor and amplification force error (linear)
$\bar{m}_e, \bar{m}_e, m_e$	Inertias of exoskeleton, load and combined (linear)	$\bar{Z}_e, \bar{Z}_e, Z_e$	Impedances of exoskeleton, load and combined (linear)
Z_{h-e}	Combined impedance of human and loaded exoskeleton (linear)	$\omega_{h-e}, \zeta_{h-e}$	Natural frequency and damping ratio of Z_{h-e}
Z_{ah-e}	Combined impedance of amplified human and loaded exoskeleton (linear)	$\omega_{ah-e}, \zeta_{ah-e}$	Natural frequency and damping ratio of Z_{ah-e}
θ_e, x_e	Exoskeleton joint angle (rotary) and position (linear)	τ_e, f_e	Environment torque (rotary) and force (linear)
k_s, Z_s	Spring stiffness and impedance (linear)	τ_s, f_s	Actuator spring torque (rotary) and force (linear)
k_{ss}, b_{ss}, Z_{ss}	Virtual spring stiffness, damping and impedance (linear)	f_r	Reference spring force (linear)
b_a, m_a, Z_a	Motor damping, inertia and impedance (linear)	f_a, f_δ	Motor and disturbance force (linear)
x_a, x_d	Motor position and position command (linear)	τ_d, f_d	Desired spring torque (rotary) and force (linear)
Z_{ss-a}	Combined impedance of virtual spring and motor (linear)	$\omega_{ss-a}, \zeta_{ss-a}$	Natural frequency and damping ratio of Z_{ss-a}
P_s, P_α	Transfer functions: from f_d to f_s , from f_d to f_α	Q, C_s, C_α	DoB filter, spring force and amplification force controller
u_h, f_{ext}	Biasing force from human and environment (linear)	C, K	Extender's position and amplification controller

admittance based, and capable of walking. However, when admittance robots interact with semi-rigid environments their interaction forces are determined by the position controller, not the human. A modified admittance scheme with position control implemented via inverse dynamics shares these fundamental limitations [19], and requires either extra force-sensors or modification to the dynamic model to carry load.

A review paper on admittance control [20] suggests employing feedback based on acceleration when possible. Acceleration feedback (and the use of accelerometers) dominate the control strategy of BLEEX [14]. And one exoskeleton has used acceleration to reduce the apparent inertia of the operator (rather than merely reducing the apparent mass of the exoskeleton) [21]. Acceleration has been proposed as a complete framework for exoskeleton control [22]. But successful as this strategy is, it cannot aid in amplification objectives—since the environment is generally not known in advance.

In one exoskeleton a simpler strategy was employed which fed contact forces to motor-current through the motion Jacobian transpose [23] (a study not on exoskeleton control but on an exoskeleton's effect on human motion). This strategy is able to amplify the human with respect to both interaction forces and exoskeleton dynamic forces, but the researchers only accomplished a modest amplification (around 2) in their study, and did not discuss the tuning of their controller.

Aiming to accomplish amplification, our exoskeleton hardware is designed to include high performance force controlled series elastic actuators [24] (similar to the force controlled actuation in [21], which was based on [25], which used a disturbance observer on motor position, while ours operates on the spring deflection). Using a series elastic actuator allows us to replicate an amplification error framework reminiscent of [12], but without a force sensor between the exoskeleton and the environment. Instead, we use the spring deflection of the elastic actuators resulting in our scheme to not only attenuate the load but also the exoskeleton dynamics. As in [10], we need to model the human as an uncertain system and check for complementary stability. However, we design our stability filter using the uncertain bode plot between desired force (sent to the SEA) and amplification error. Following the arguments laid out in

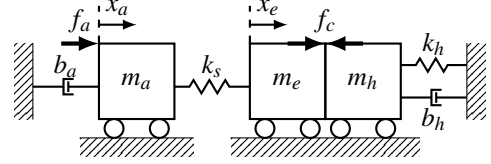


Fig. 1: A mass-damper-spring model of the human, exoskeleton and SEA.

[10], and the additional examples in [26], [8], we employ a single-DOF system to study the simplest possible case of amplification exoskeletons. The non-trivial extension to multi-joint systems remains as future work.

II. MODELING

Fig. 1 introduces our model of the human–exoskeleton–actuator system, which incorporates a reflection of rotational human elbow motions into a prismatic motion reference frame. We define the human forearm moment of inertia M_h , elbow damping B_h , elbow stiffness K_h and loaded exoskeleton moment of inertia $M_e = \bar{M}_e + \bar{M}_e$ (including exoskeleton moment of inertia \bar{M}_e and load moment of inertia \bar{M}_e) as parameters in the rotary joint space. Actuator spring stiffness k_s , actuator inertia m_a , and actuator damping b_a are parameters in the linear actuator space—with the inertia and damping of the motor rotor being transformed into m_a and b_a in the actuator space by the drive train transmission ratio.

Motor force, f_a , is the input. Spring force f_s , contact torque τ_c —obtained using a six-axis force sensor at the human–robot interface and cast as a torque using the motion Jacobian transpose—, and exoskeleton joint position θ_e are available from sensors. The force from the load to the exoskeleton is not measured but defined as τ_e in the joint space. Linear versions of rotary position variables are defined based on the joint-angle-dependent inverse kinematics: linear actuator position x_a , and linear exoskeleton position x_e . We use the joint-angle-dependent transmission ratio $r(\theta_e) : 1$ to define linear versions of the rotational space parameters: $m_h = M_h/r(\theta_e)^2$, $b_h = B_h/r(\theta_e)^2$, $k_h = K_h/r(\theta_e)^2$, $\bar{m}_e = \bar{M}_e/r(\theta_e)^2$, $\bar{m}_e = \bar{M}_e/r(\theta_e)^2$, $m_e = \bar{m}_e + \bar{m}_e$, $f_c = \tau_c/r(\theta_e)$ and $f_e = \tau_e/r(\theta_e)$. See list of symbols in Tab. I.

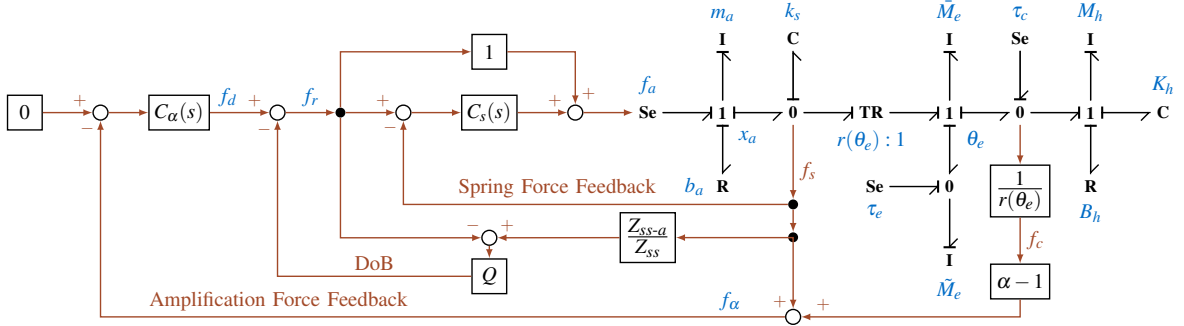


Fig. 2: Block diagram of spring force feedback, DoB and amplification force feedback. Dynamics of human, exoskeleton and SEA are represented as a bond graph with effort sources f_a , τ_c and τ_e .

A. Human-Exoskeleton-Actuator Interaction

We model the impedance of the human as in [10],

$$Z_h = f_c/\dot{x}_e = m_h s + b_h + k_h s^{-1}, \quad (1)$$

and the impedance of the unloaded exoskeleton, the load and the loaded exoskeleton,

$$\bar{Z}_e = (f_s - f_c - f_e)/\dot{x}_e = \bar{m}_e s, \quad \tilde{Z}_e = f_e/\dot{x}_e = \tilde{m}_e s, \quad (2)$$

$$Z_e = (f_s - f_c)/\dot{x}_e = \bar{Z}_e + \tilde{Z}_e = m_e s,$$

Together in series,

$$Z_{h-e} = Z_h + Z_e = f_s/\dot{x}_e, \quad (3)$$

represents a system in parallel with the elastic actuator.

Considering the impedance of the spring,

$$Z_s = f_s/(\dot{x}_a - \dot{x}_e) = k_s s^{-1}, \quad (4)$$

and the impedance of the motor,

$$Z_a = (f_a - f_s)/\dot{x}_a = m_a s + b_a, \quad (5)$$

motion of the whole system relates to the required input force,

$$\frac{f_a}{\dot{x}_e} = Z_{h-e} + \frac{(Z_{h-e} + Z_s) \cdot Z_a}{Z_s}. \quad (6)$$

This provides a human-dependent force-control plant,

$$\frac{f_s}{f_a} = \frac{Z_{h-e} \cdot Z_s}{Z_{h-e} \cdot Z_s + (Z_{h-e} + Z_s) \cdot Z_a}. \quad (7)$$

B. Spring Force Control

Under the spring force control shown in Fig. 2's block diagram bond graph,

$$f_a = f_r + C_s(s) \cdot (f_r - f_s), \quad (8)$$

where f_r is the reference spring force and $C_s(s)$ is a PD controller. Combining (7) and (8),

$$\frac{f_s}{f_r} = \frac{Z_{h-e} \cdot Z_{ss}}{Z_{h-e} \cdot Z_{ss} + (Z_{h-e} + Z_s) \cdot Z_a}, \quad (9)$$

where $Z_{ss} = Z_s \cdot [1 + C_s(s)] = b_{ss} + k_{ss} s^{-1}$ is the virtual impedance of spring. By tuning the PD gains of $C_s(s)$, the virtual spring stiffness of k_{ss} and the virtual spring damping b_{ss} can be modified.

If Z_{h-e} is infinitely large, (9) simplifies to,

$$\frac{f_s}{f_r} = \frac{Z_{ss}}{Z_{ss-a}}, \quad (10)$$

where $Z_{ss-a} = Z_{ss} + Z_a$ is the combined impedance of the virtual spring and the actuator.

Under the disturbance observer (DoB) of [24],

$$f_r = f_d - [Q \cdot \frac{Z_{ss-a}}{Z_{ss}} \cdot f_s - Q \cdot f_r], \quad (11)$$

where f_d is the DoB spring force command and Q is a low-pass filter of sufficient order to ensure the observer is causal (2nd order in our analytical model, but 4th order in the low level firmware).

Combining (9) and (11), we obtain a transfer function $P_s(s)$ from f_d to f_s ,

$$P_s(s) = \frac{f_s}{f_d} = \frac{Z_{h-e} \cdot Z_{ss}}{Z_{h-e} \cdot Z_{ss} + [Z_{h-e} + (1-Q) \cdot Z_s] \cdot Z_a}. \quad (12)$$

By tuning the cut-off frequency of Q , (10) is (approximately) enforced without an infinitely large Z_{h-e} —as explained in [24], this approximation depends on a load inertia lower-bound (in our case, the exoskeleton inertia).

III. LOOP SHAPING

Fig. 3 shows the amplification exoskeleton concept in comparison with the extender concept of [12]. We define the goal of an amplification exoskeleton to be reduction of both environmental and exoskeleton-dynamic load experienced by the user. This differs from an extender, which only seeks to reduce environmental forces—leaving the exoskeleton to be handled by position control. In the extender, drive-train disturbance forces (from stick-slip friction and potentially nonbackdrivable gearing) f_δ are attenuated by position control, while in our system they are attenuated by the DoB. Another important difference is our use of the f_s signal in place of f_e ; the two are related through

$$x_e = \frac{1}{\bar{Z}_e s} (f_s - f_e - f_c), \quad (13)$$

$$f_e + \bar{Z}_e s \cdot x_e = f_s - f_c, \quad (14)$$

which means that when we replace [12]'s feedback of f_e with feedback of f_s , we must adjust α by -1 and expect this new controller to attenuate the exoskeleton's own impedance in addition to attenuating environmental forces.

A. Plant of Human Force Amplification

We define an amplification error signal $f_\alpha = (\alpha - 1)f_c + f_s$, and consider the transfer function $P_\alpha(s)$ (obtained by

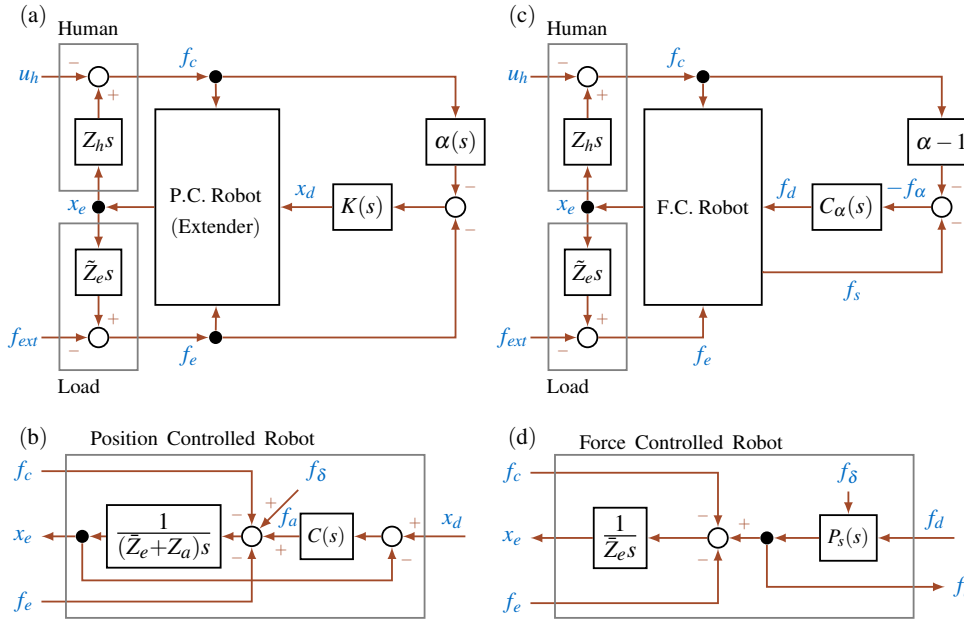


Fig. 3: Relation between extender concept (a) of [12], which used a position controlled robot (b) as the “extender” plant, and our concept of the amplification exoskeleton (c) based on a series elastic actuated, force controlled robot (d).

combining (1), (3) and (12)) from the desired force f_d to the error f_α ,

$$P_\alpha(s) = \frac{f_\alpha}{f_d} = \frac{Z_{\alpha h-e} \cdot Z_{ss}}{Z_{h-e} \cdot Z_{ss} + [Z_{h-e} + (1-Q) \cdot Z_s] \cdot Z_a}, \quad (15)$$

where $Z_{\alpha h-e} = \alpha Z_h + Z_e$ is the combined impedance of the amplified human and exoskeleton.

Because the cut-off frequency of Q is much larger than the natural frequency of the human system, $\omega_h = \sqrt{k_h/m_h}$, and the natural frequency of the force control, $\omega_{ss-a} = \sqrt{k_{ss}/m_a}$, $P_\alpha(s)$ can be approximated:

$$P_\alpha(s) \approx \frac{Z_{\alpha h-e} \cdot Z_{ss}}{Z_{h-e} \cdot Z_{ss-a}}. \quad (16)$$

As shown in Fig. 4—assuming k_{ss}/b_{ss} is high enough to ignore— $P_\alpha(s)$ has a pair of conjugate zeros at $\omega_{\alpha h-e} = \sqrt{k_h/(m_e/\alpha + m_h)}$ and two pairs of conjugate poles at $\omega_{h-e} = \sqrt{k_h/(m_e + m_h)}$ and at ω_{ss-a} . ω_{ss-a} is usually larger than the maximum of ω_h . However, even if an actuator has a soft serial spring or a huge motor rotor inertia, increasing the gain of $C_s(s)$ will result in an ω_{ss-a} much larger than ω_{h-e} and $\omega_{\alpha h-e}$ —which avoids the phase drop below -180° in $P_\alpha(s)$.

The bode magnitude plot of $P_\alpha(s)$ starts from $20 \log(\alpha)$ dB in steady state. If the loop of $P_\alpha(s)$ is directly closed, the gain cross-over is decided by the feedback gain—and of course by the shape of $P_\alpha(s)$, which varies with the value of α , the stiffness and damping of the human, and the environmental impedance.

When α is set very close to 1 the actuator does almost no amplification, and $P_\alpha(s)$ approaches the closed loop force tracking behavior of the low-level force controller—in this configuration $\omega_{\alpha h-e}$ converges to ω_{h-e} and $P_\alpha(s)$ looks like a second order low pass filter.

On the other hand, as α increases, $\omega_{\alpha h-e}$ travels right, and the gap between ω_{h-e} and $\omega_{\alpha h-e}$ widens. This gap behaves

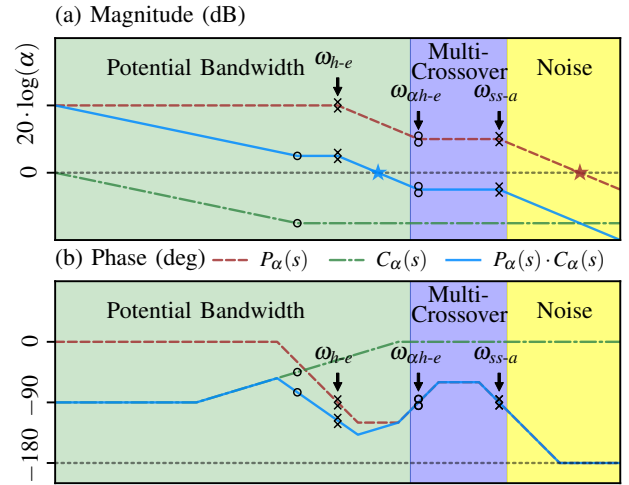


Fig. 4: Conceptual bode plots with a large k_{ss}/b_{ss} show the plant $P_\alpha(s)$, PI compensator $C(s)$, and compensated open-loop. Regions are color-coded: the green region has practical model-accuracy, the blue region reflects the multi-crossover behavior which makes a compensator design unreliable, and the yellow region is noise dominated in our identification tests, so the model is unreliable. Crosses, circles and stars indicate the poles, zeros and cross-over points.

like a second order lag compensator—and it corresponds to a phase dip that approaches -180° as the gap widens.

When the human stiffness is very low, both ω_{h-e} and $\omega_{\alpha h-e}$ shift to lower frequencies together—unless there is an environmental stiffness. If the human becomes stiffer the two shift higher together as well.

Fig. 4 highlights three frequency bands. At the highest frequencies, it should be possible to design controllers, but on our hardware the amount of amplified noise makes them

to dangerous to try. In the next highest band it is very easy to gain two extra cross-overs, because the zeros at $\omega_{\alpha h-e}$ are under damped. The lowest frequency region is where we will attempt to cross over in this paper.

B. Amplification Force Control

By adding a proportional gain k_p less than 1 to $P_\alpha(s)$, the cross-over shifts below $\omega_{\alpha h-e}$. However, It also reduces the low frequency magnitude and increases the closed loop steady state error. An integral term can be added to boost the low frequency magnitude while maintaining the same cross-over below $\omega_{\alpha h-e}$. We parameterize a simple PI controller transfer function $C_\alpha(s)$ (from $-f_\alpha$ to f_d in Fig. 2) as

$$C_\alpha(s) = k_p \cdot \frac{s+z}{s}, \quad (17)$$

where z is a zero with $k_p \cdot z$ as the integral gain. As a reference, $k_p = \frac{1}{\alpha}$ starts the compensated open-loop plant at a low frequency gain equal to unity.

The amplification tracking is evaluated by comparing $-\frac{f_s}{f_c}$ to $\alpha - 1$. The transfer function from $-(\alpha - 1)f_c$ to f_s is equivalent to closing the loop of $C_\alpha(s)P_s(s)$. Because the cut-off frequency of Q is much greater than ω_{ss-a} , $C_\alpha(s)P_s(s)$ can be simplified as

$$C_\alpha(s)P_s(s) \approx k_p \cdot \frac{s+z}{s} \cdot \frac{Z_{ss}}{Z_{ss-a}}. \quad (18)$$

Notice that $\frac{Z_{ss}}{Z_{ss-a}}$ behaves as a low-pass filter with a cut-off frequency at ω_{ss-a} . Therefore, $C_\alpha(s)P_s(s)$ is dominated by $C_\alpha(s)$ at low frequency. This allows the amplification tracking to be deterministic despite the uncertainty from Z_{h-e} .

The dynamic tracking of amplification depends a lot on the location of z in $C_\alpha(s)$ and the magnitude of $C_\alpha(s)P_s(s)$. However, z cannot be arbitrarily large because it allows $C_\alpha(s)$ to drop more phase from P_α between ω_{h-e} and $\omega_{\alpha h-e}$.

IV. SYSTEM IDENTIFICATION

The experiments in this section use the elbow-joint exoskeleton testbed (Fig. 5(a)) with a SEA and a contact sensor. The SEA includes a spring of $k_s = 796958 \text{ N/m}$ and a motor of $m_a = 250 \text{ kg}$ and $b_a = 4500 \text{ Ns/m}$. The aluminum exoskeleton arm has $\bar{M}_e = 0.1 \text{ kgm}^2$ and $r(\theta_e)$ in the range of $[0.005, 0.025] \text{ m}$.

A. Chirp Signal Experiments

The human model identification (Fig. 5(b)) includes four chirp signal experiments (Exp. IV-A.1-4) with a 27-year old male subject. The subject wears the cuff of the contact sensor and straps his upper arm to a fixed mount. A 300 second, exponential chirp signal is provided as a torque command to the low level force controller. The subject tries to hold the exoskeleton still—with various levels of attempted stiffness—as the exoskeleton vibrates. The exoskeleton does not hit its joint safety hard-stops in these experiments, and operator has access to the system emergency stop at all times.

The time domain data (spring torque $\tau_s = f_s \cdot r(\theta_e)$ and angle θ_e) from the experiments are used to form a frequency response function representing the human plus the exoskeleton (Figs. 6 and 7). The value of M_h is identified by the

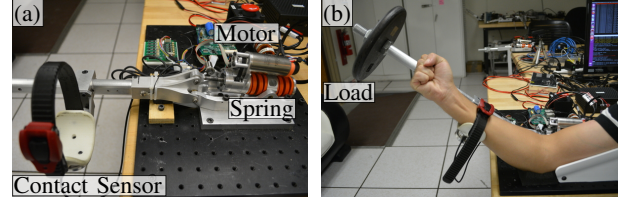


Fig. 5: An elbow-joint exoskeleton testbed (a) is used for a human model identification experiment (b).

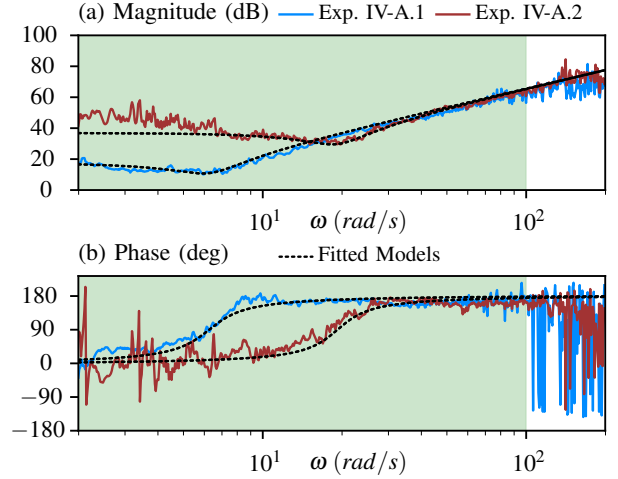


Fig. 6: Bode plots of $\tau_s/\theta_e(s)$, data and fitted models, for Exp. IV-A.1 and Exp. IV-A.2. Only the green highlighted region is used for identifying B_h and K_h with regressions.

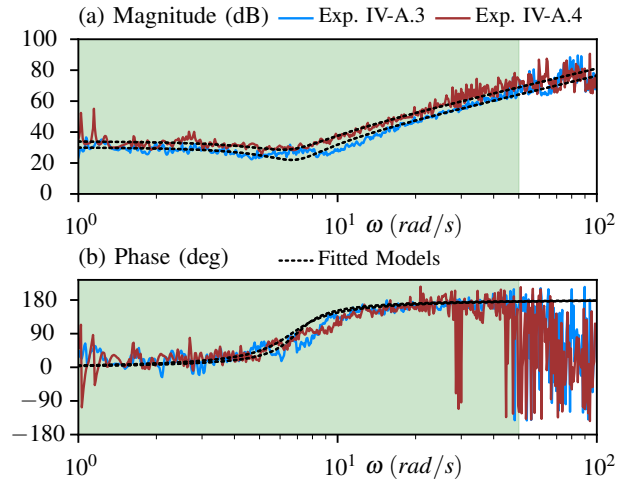


Fig. 7: Bode plots of $\tau_s/\theta_e(s)$, data and fitted models, for Exp. IV-A.3 and Exp. IV-A.4. Only the green highlighted region is used for identifying B_h and K_h with regressions.

TABLE II: Empirical Human Impedance Parameters

Experiment	$K_h (\frac{Nm}{rad})$	$B_h (\frac{Nms}{rad})$	$M_h + M_e (kgm^2)$	ζ_{h-e}	$ \tau_d (Nm)$
Exp. IV-A.1	7.44	0.56	0.09 + 0.10	0.24	2.0
Exp. IV-A.2	70.11	1.60	0.09 + 0.10	0.22	5.0
Exp. IV-A.3	31.91	1.84	0.09 + 0.57	0.20	4.0
Exp. IV-A.4	50.18	4.21	0.09 + 1.05	0.28	4.0

asymptotic behavior at high frequency and the value of B_h and K_h are identified by regressions with identified inertia.

B. Human Joint Stiffness and Damping

The joint stiffness is decided by contractions in the group of muscles around the joint. By activating a higher level of contractions in flexor and extensor of elbow, the elbow stiffness can be increased [27]. Exp. IV-A.1 and Exp. IV-A.2 identify the range of subject's elbow K_h (Fig. 6). The muscle around the elbow is as relaxed as possible in Exp. IV-A.1 and fully tensed in Exp. IV-A.2. The subject clenches his hand into a fist to help him achieve a high stiffness and leaves it open for soft behavior. This is also a convenient way to visually distinguish these two types of human behavior in the rest of this paper.

Although the stiffness of a human elbow can possibly go up to 400 Nm/rad , such stiffness is only possible with a perturbation of 40 Nm [28]. The chirp amplitude $|\tau_d|$ is only 2 Nm in Exp. IV-A.1 and 5 Nm in Exp. IV-A.2 to provide just enough perturbation of torque while the subject can still keep the exoskeleton within the safety joint limits. The results from Exp. 1-2 suggest that K_h varies within the $[7.44, 70.11] \text{ Nm/rad}$ range.

Without additional inertia added to the exoskeleton and load, the human is able to maintain an invariant damping ratio of the arm [29]. However, the human is also able to adapt damping and stiffness to compensate the environment dynamics [30]. We added a 5 lb and a 10 lb loads at 18 inches from the joint on the exoskeleton in Exp. IV-A.3 and Exp. IV-A.4 (Fig. 7). The results from the four experiments suggest that the human tends to maintain an invariant damping ratio ζ_{h-e} of Z_{h-e} when wearing the exoskeleton (Tab. II). Therefore, we model the human as a 1-parameter system. With changing values of K_h and M_e , we predict B_h

$$B_h = 2\zeta_{h-e}\sqrt{K_h(M_h + M_e)}. \quad (19)$$

The identified values of K_h , B_h and M_h (Tab. II) suggest the value of ζ_{h-e} of the subject is around 0.23.

V. VALIDATION

Considering the range of K_h , m_e and $r(\theta_e)$, a model of $P_\alpha(s)$ with uncertainty can be obtained and used for PI controller design for $\alpha = 10$. In this section, an aggressive controller and a robust controller are implemented to validate the uncertain model and control strategy. $C_s(s)$ is set with $k_{ss} = 2k_s$ and $b_{ss} = 0.039k_s$ to achieve a high natural frequency and damping ratio of Z_{ss-a} . The cut-off frequency of Q is set to be 40 Hz. The video of all the experiments in this section is available at <https://www.youtube.com/watch?v=EUHoAEwCfFY>.

A. Aggressive Controller

A controller with $k_p = 0.1$ and $z = 30$ is implemented with a load of 10 lb on the exoskeleton, the uncertain model suggests it makes the exoskeleton slightly unstable with a low value of K_h but fully stable with a high value of K_h (Fig. 8).

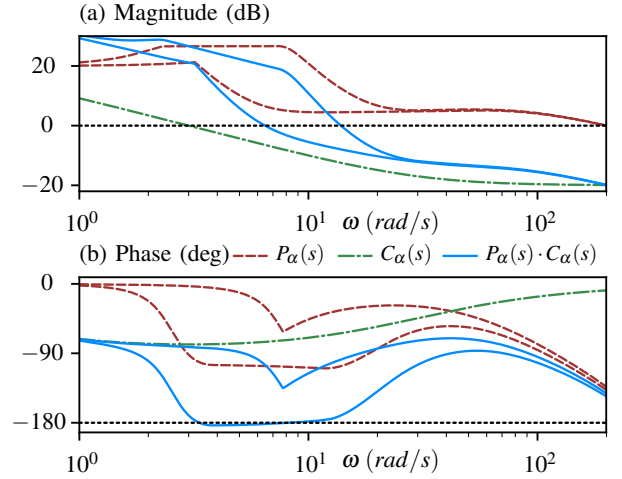


Fig. 8: Uncertain model of $P_\alpha(s)$ is made by 20 interpolations of K_h in the range of $[7.44, 70.11] \text{ Nm/rad}$ and 5 interpolations of $r(\theta_e)$ in the range of $[0.005, 0.025] \text{ m}$. M_e is $1.05 \text{ kg} \cdot \text{m}^2$. Time delay is 6 ms.

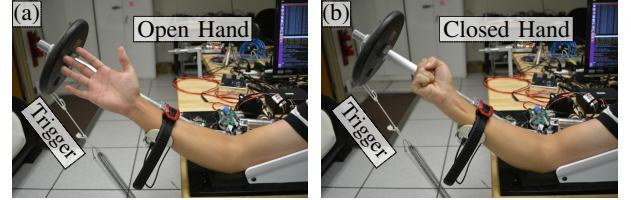


Fig. 9: Step response with an aggressive controller was triggered by releasing an external spring at the end of the exoskeleton arm. The subject opens (a) (Exp. V-A.1) and closes (b) (Exp. V-A.2) his hand to illustrate different levels of muscle co-contraction (and therefore stiffness).

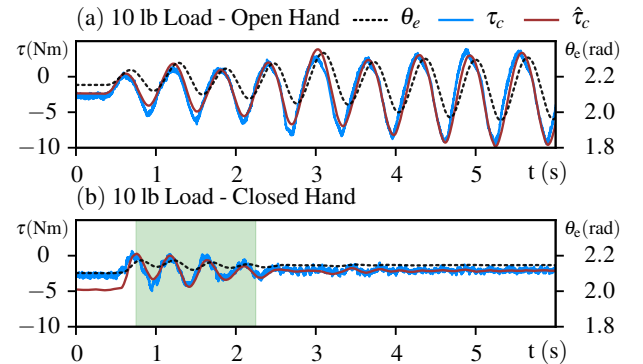


Fig. 10: Step response results: Exp. V-A.1 (a) and Exp. V-A.2 (b). Because motion settles down early in (b), only the green highlighted region is used for estimating \hat{B}_h and \hat{K}_h .

TABLE III: Estimated Parameters in Exp. V-A-series

Experiment	Load (lb)	Hand	$\hat{K}_h (\frac{\text{Nm}}{\text{rad}})$	$\hat{B}_h (\frac{\text{Nms}}{\text{rad}})$	$\hat{\zeta}_{h-e}$
Exp. V-A.1	10	open	27.12	2.34	0.22
Exp. V-A.2	10	closed	59.34	3.99	0.25

To validate this prediction, the subject wearing the exoskeleton with the controller either opens his hand—for low values of K_h —or tightly closes his hand—for high stiffness K_h —in two separate experiments: Exp. V-A.1 and Exp. V-A.2 respectively. A spring with one end connected on the ground and the other end hanging on the end of the exoskeleton is released at the beginning of each experiment—a step input in external force (Fig. 9).

The experiment results (Fig. 10) show that the exoskeleton joint oscillates with a slowly increasing amplitude with open hand and oscillates but settles down in 2 seconds with closed hand. By using the data of τ_c , θ_e and $\dot{\theta}_e$, a linear regression is built to identify a simplified human model with only damping \hat{B}_h and stiffness \hat{K}_h (Tab. III). The value of \hat{K}_h verifies that human maintains a much higher stiffness with closed hand than open hand. The estimated contact torques $\hat{\tau}_c = \hat{B}_h \dot{\theta}_e + \hat{K}_h \theta_e$ are well matched to the measured τ_c (Fig. 10)—which confirms that the system is oscillating despite a passive, spring-damper-like, human behavior. The estimated damping ratio $\hat{\zeta}_{h-e} = \hat{B}_h / (2\sqrt{\hat{K}_h M_e})$ for open hand is slightly lower than 0.23 and makes the system more unstable than the prediction.

B. Robust Controller

We also implemented a controller with $k_p = 0.1$ and $z = 10$ for improved robustness to parameter variation in the exoskeleton load, and human stiffness (and damping). The uncertain model suggests it maintains a phase margin no less than 10° for permissible values of K_h , M_e , and $r(\theta_e)$ (Fig. 11).

To validate the expectation, the experiments include two different M_e (with 0 and 10 lb load) and two different K_h (open and closed hands). The subject generates motion with 0.1 Hz trapezoid-like wave for steady state tests and 1 Hz sinusoid-like wave for dynamic tests. We refer to these eight experiments as the Exp. V-B-series.

The integrator in the controller is implemented as a pole $p = 0.01$ to numerically integrate f_α . Because the amplification tracking relies mostly on $C_\alpha(s)$, a static gain of 8.18 and a 1 Hz dynamic gain of 1.42 with phase shift of -56.94° are expected for $-f_s/f_c$ (or $-\tau_s/\tau_c$ in joint space).

The experiment results (Fig. 12) verify that the exoskeleton is stable with all eight settings. The values of gain and phase shift are also close to the expected values (Tab. IV). The results show little influence on amplification tracking from the variation of Z_h and M_e , as expected.

VI. DISCUSSION

Amplification exoskeletons, seeking to amplify the strength of the human as it interacts both with the environment and the inertia of the robot itself, represent a different strategy of human augmentation compared to the extender concept of [12]. Series elastic actuators fit into the structure of amplification exoskeleton by incorporating a direct measurement of actuator force through spring deflection and an accurate actuator force control (with a disturbance observer).

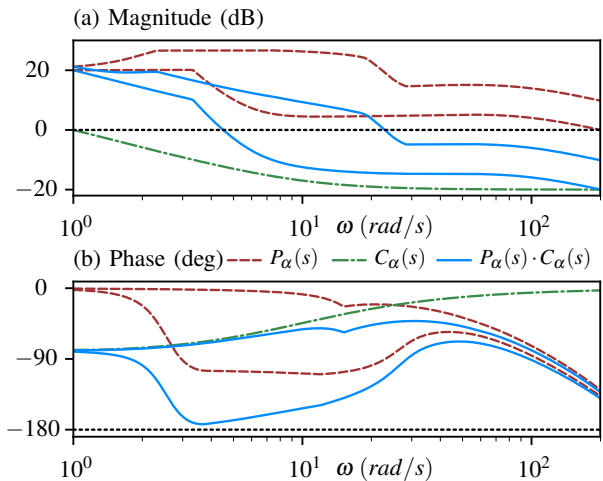


Fig. 11: Uncertain model of $P_\alpha(s)$ is made by 20 interpolations of K_h in the range of $[7.44, 70.11] \text{ Nm/rad}$, 20 interpolations of M_e in the range of $[0.1, 1.05] \text{ kg}\cdot\text{m}^2$, and 5 interpolations of $r(\theta_e)$ in the range of $[0.005, 0.025] \text{ m}$. Time delay is 6 ms.

TABLE IV: Observed Amplification in Exp. V-B-series

Load (lb)	Hand	$ \frac{\tau_s}{\tau_c} $ (static)	$ \frac{\tau_s}{\tau_c} $ (1Hz)	$\angle -\frac{\tau_s}{\tau_c}$ (1Hz)
0	open	8.15	1.48	-53.55°
0	closed	8.05	1.49	-53.68°
10	open	8.13	1.58	-53.39°
10	closed	8.18	1.46	-50.75°

We showcase a proportional-integral amplification force controller which aims to stably achieve high steady-state amplification tracking performance and a large amplification factor. Since an aggressive controller (with a high zero frequency z) causes stability problem in the case of low human joint stiffness, our results with a robust controller corroborate [10] in demonstrating that the variability in human stiffness must be accounted for in designing the controller. Our control strategy leaves exoskeleton designers with a trade-off between high amplification factors, high bandwidth of the amplification error attenuation function, and accurate knowledge of the human stiffness limits.

Our strategy can potentially be extended to multi-DOF cases by projecting the human-exoskeleton interaction forces measured from the contact sensors to each joint space and developing joint level amplification force controllers accordingly. Actuator force saturation may appear on amplification exoskeletons with other human joints (especially those at the lower limbs) where higher maximum joint torques can exist. This saturation problem can be considered as a reduction of the actual amplification factor and certainly reduces the bandwidth and crossover frequency of force amplification. Nevertheless, a decrease in crossover frequency (as discussed on Fig. 4) does not create an additional stability issue for our proportional-integral controller.

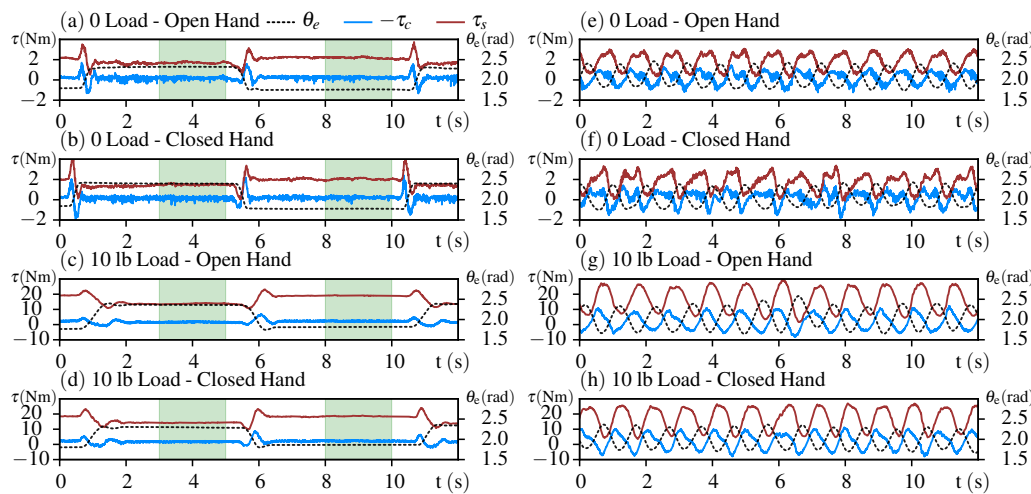


Fig. 12: Results from the eight Exp. V-B-series tests. Steady state tests (a)-(d) and dynamic tests (e)-(h) are processed from the subject. Only data in the green highlighted regions are used for calculating the static gain.

REFERENCES

- [1] A. M. Dollar and H. Herr, "Lower extremity exoskeletons and active orthoses: challenges and state-of-the-art," *IEEE Transactions on Robotics*, vol. 24, no. 1, pp. 144–158, 2008.
- [2] H. Herr, "Exoskeletons and orthoses: classification, design challenges and future directions," *Journal of Neuroengineering and Rehabilitation*, vol. 6, no. 1, p. 21, 2009.
- [3] S. Lee, J. Kim, L. Baker, A. Long, N. Karavas, N. Menard, I. Galiana, and C. J. Walsh, "Autonomous multi-joint soft exosuit with augmentation-power-based control parameter tuning reduces energy cost of loaded walking," *Journal of Neuroengineering and Rehabilitation*, vol. 15, no. 1, p. 66, 2018.
- [4] H. Kazerooni, "Human-robot interaction via the transfer of power and information signals," *IEEE Transactions on Systems, Man, and Cybernetics*, vol. 20, no. 2, pp. 450–463, 1990.
- [5] N. Hogan, "Adaptive control of mechanical impedance by coactivation of antagonist muscles," *IEEE Transactions on Automatic Control*, vol. 29, no. 8, pp. 681–690, 1984.
- [6] J. E. Colgate and N. Hogan, "Robust control of dynamically interacting systems," *International Journal of Control*, vol. 48, no. 1, pp. 65–88, 1988.
- [7] N. Hogan, "Controlling impedance at the man/machine interface," in *Robotics and Automation (ICRA), 1989 IEEE International Conference on*. IEEE, 1989, pp. 1626–1631.
- [8] J. E. Colgate and J. M. Brown, "Factors affecting the z-width of a haptic display," in *Robotics and Automation (ICRA), 1994 IEEE International Conference on*. IEEE, 1994, pp. 3205–3210.
- [9] R. J. Adams and B. Hannaford, "Stable haptic interaction with virtual environments," *IEEE Transactions on Robotics and Automation*, vol. 15, no. 3, pp. 465–474, 1999.
- [10] S. P. Buerger and N. Hogan, "Complementary stability and loop shaping for improved human-robot interaction," *IEEE Transactions on Robotics*, vol. 23, no. 2, pp. 232–244, 2007.
- [11] J. B. Makinson, D. P. Bodine, and B. R. Fick, "Machine augmentation of human strength and endurance Hardiman I prototype project," Specialty Materials Handling Products Operation, General Electric Company, Tech. Rep., 1969.
- [12] H. Kazerooni and J. Guo, "Human extenders," *Journal of Dynamic Systems, Measurement, and Control*, vol. 115, no. 2B, pp. 281–290, 1993.
- [13] H. Kazerooni, J.-L. Racine, L. Huang, and R. Steger, "On the control of the berkeley lower extremity exoskeleton (bleex)," in *Robotics and Automation (ICRA), 2005 IEEE International Conference on*. IEEE, 2005, pp. 4353–4360.
- [14] H. Kazerooni, "Exoskeletons for human power augmentation," in *Intelligent Robots and Systems (IROS), 2005 IEEE/RSJ International Conference on*. IEEE, 2005, pp. 3459–3464.
- [15] A. Lecours, B. M. St-Onge, and C. Gosselin, "Variable admittance control of a four-degree-of-freedom intelligent assist device," in *Robotics and Automation (ICRA), 2012 IEEE International Conference on*. IEEE, 2012, pp. 3903–3908.
- [16] W. Yu and J. Rosen, "Neural pid control of robot manipulators with application to an upper limb exoskeleton," *IEEE Transactions on Cybernetics*, vol. 43, no. 2, pp. 673–684, 2013.
- [17] M. Fontana, R. Vertechy, S. Marcheschi, F. Salsedo, and M. Bergamasco, "The body extender: A full-body exoskeleton for the transport and handling of heavy loads," *IEEE Robotics & Automation Magazine*, vol. 21, no. 4, pp. 34–44, 2014.
- [18] S. C. Jacobsen and M. X. Olivier, "Contact displacement actuator system," Sep. 30 2014, US Patent 8,849,457.
- [19] H.-D. Lee, B.-K. Lee, W.-S. Kim, J.-S. Han, K.-S. Shin, and C.-S. Han, "Human-robot cooperation control based on a dynamic model of an upper limb exoskeleton for human power amplification," *Mechatronics*, vol. 24, no. 2, pp. 168–176, 2014.
- [20] A. Q. Keemink, H. van der Kooij, and A. H. Stienen, "Admittance control for physical human-robot interaction," *The International Journal of Robotics Research*, 2017.
- [21] K. Kong and M. Tomizuka, "Control of exoskeletons inspired by fictitious gain in human model," *IEEE/ASME Transactions on Mechatronics*, vol. 14, no. 6, pp. 689–698, 2009.
- [22] T. Boaventura and J. Buchli, "Acceleration-based transparency control framework for wearable robots," in *Biomedical Robotics and Biomechanics (BioRob), 2016 IEEE International Conference on*. ETH Zürich, 2016.
- [23] D. Zanutto, Y. Akiyama, P. Stegall, and S. K. Agrawal, "Knee joint misalignment in exoskeletons for the lower extremities: Effects on user's gait," *IEEE Transactions on Robotics*, vol. 31, no. 4, pp. 978–987, 2015.
- [24] N. Paine, S. Oh, and L. Sentis, "Design and control considerations for high-performance series elastic actuators," *IEEE/ASME Transactions on Mechatronics*, vol. 19, no. 3, pp. 1080–1091, 2014.
- [25] K. Kong, J. Bae, and M. Tomizuka, "Control of rotary series elastic actuator for ideal force-mode actuation in human-robot interaction applications," *IEEE/ASME Transactions on Mechatronics*, vol. 14, no. 1, pp. 105–118, 2009.
- [26] H. Kazerooni and T. J. Snyder, "Case study on haptic devices: Human-induced instability in powered hand controllers," *Journal of Guidance, Control, and Dynamics*, vol. 18, no. 1, pp. 108–113, 1995.
- [27] S. C. Cannon and G. I. Zahalak, "The mechanical behavior of active human skeletal muscle in small oscillations," *Journal of Biomechanics*, vol. 15, no. 2, pp. 111–121, 1982.
- [28] J. M. Lanman, "Movement and the mechanical properties of the intact human elbow joint." Ph.D. dissertation, Massachusetts Institute of Technology, 1980.
- [29] E. J. Perreault, R. F. Kirsch, and P. E. Crago, "Multijoint dynamics and postural stability of the human arm," *Experimental Brain Research*, vol. 157, no. 4, pp. 507–517, 2004.
- [30] T. E. Milner and C. Cloutier, "Compensation for mechanically unstable loading in voluntary wrist movement," *Experimental Brain Research*, vol. 94, no. 3, pp. 522–532, 1993.